

Generation of optical pulses in VCSELs below the static threshold using asymmetric current modulation

J. Zamora-Munt and C. Masoller

*Departament de Física i Enginyeria Nuclear, Universitat Politècnica de Catalunya, Colom 11,
E-08222 Terrassa, Barcelona, Spain*

jordi.zamora.munt@upc.edu; cristina.masoller@upc.edu

Abstract: We present a novel method for the generation of sub-nanosecond optical pulses in directly modulated vertical-cavity surface-emitting lasers (VCSELs) that operate, on average, below the cw threshold. Using the spin-flip model we demonstrate that irregular optical pulses in two orthogonal linear polarizations can be generated via asymmetric triangular modulation of period of a few nanoseconds, with a slow rising ramp followed by a fast decreasing one. For an optimal modulation asymmetry the effective threshold reduction is about 20%, the pulse amplitude is maximum and the dispersion of the pulse amplitude is minimum.

© 2008 Optical Society of America

OCIS codes: (250.7260) Vertical cavity surface emitting lasers; (270.3100) Instabilities and chaos; (140.3430) Laser theory

References and links

1. K. Iga, "Surface-emitting laser -its birth and generation of new optoelectronics field," IEEE J. Sel. Top. Quantum Electron. vol. **6**, pp. 1201-1215, Sep.-Oct. (2000).
2. *VCSELs and Optical Interconnects*, H. Thienpont and J. Danckaert, eds., SPIE Proc. vol. 4942, (2003).
3. A. J. Danner, J. J. Raftery, P. O. Leisher, and K. D. Choquette, "Single mode photonic crystal vertical cavity lasers," Appl. Phys. Lett. **88**, 091114 (2006).
4. T. Czynszanowski, M. Dems, and K. Panajotov, "Single mode condition and modes discrimination in photonic-crystal 1.3 μm AlInGaAs/InP VCSEL," Opt. Express **15**, 5604-5609 (2007).
5. S. Boutami, B. Benbakir, J. L. Leclercq, and P. Viktorovitch, "Compact and polarization controlled 1.55 μm vertical-cavity surface-emitting laser using single-layer photonic crystal mirror," Appl. Phys. Lett. **91** 071105 (2007).
6. C. J. Chang-Hasnain, J. P. Harbison, G. Hasnain, A. C. Vonlehmen, L. T. Florez and N. G. Stoffel, "Dynamic, polarization and transverse-mode characteristics of vertical cavity surface emitting lasers," IEEE J. Quantum Electron. **27**, 1402-1409 (1991).
7. K. D. Choquette, R. P. Schneider, K. L. Lear and R. E. Leibenguth, "Gain-dependent polarization properties of vertical-cavity lasers," IEEE J. Sel. Top. Quantum Electron. **1**, 661-666 (1995).
8. J. S. Gustavsson, A. Haglund, J. A. Vukusic, J. Bengtsson, P. Jedrasik, and A. Larsson, "Efficient and individually controllable mechanisms for mode and polarization selection in VCSELs, based on a common, localized, sub-wavelength surface grating," Opt. Express **13**, 6626-6634 (2005).
9. M. C. Y. Huang, Y. Zhou, and C. J. Chang-Hasnain, "A surface-emitting laser incorporating a high-index-contrast subwavelength grating," Nature Photonics **1**, 119-122 (2007)
10. M. C. Y. Huang, Y. Zhou, and C. J. Chang-Hasnain, "A nanoelectromechanical tunable laser," Nature Photonics **2**, 180-184 (2008).
11. G. P. Agrawal, "Effect of gain nonlinearities on period doubling and chaos in directly modulated semiconductor-lasers," Appl. Phys. Lett. **49**, 1013-1015 (1986).
12. S. Bennett, C. M. Snowden and S. Iezekiel, "Nonlinear dynamics in directly modulated multiple-quantum-well laser diodes," IEEE J. Quantum Electron. **33**, 2076-2083 (1997).

13. H. Lamela, G. Carpintero, and F. J. Mancebo, "Period tripling and chaos in the dynamic behavior of directly modulated diode lasers," *IEEE J. Quantum Electron.* **34**, 1797-1801 (1998).
14. A. Valle, L. Pesquera, S. I. Turovets, and J. M. Lopez, "Nonlinear dynamics of current-modulated vertical-cavity surface-emitting lasers," *Opt. Commun.* **208**, 173-182 (2002).
15. M. Sciamanna, A. Valle, P. Megret, M. Blondel, and K. Panajotov, "Nonlinear polarization dynamics in directly modulated vertical-cavity surface-emitting lasers," *Phys. Rev. E* **68**, 016207 (2003).
16. A. Valle, M. Sciamanna, and K. Panajotov, "Nonlinear dynamics of the polarization of multitransverse mode vertical-cavity surface-emitting lasers under current modulation," *Phys. Rev. E* **76**, 046206 (2007).
17. A. Valle, M. Sciamanna, and K. Panajotov, "Irregular pulsating polarization dynamics in gain-switched vertical-cavity surface-emitting lasers," *IEEE J. Quantum Electron.* **44**, 136-143 (2008).
18. C. Masoller, M. S. Torre, and K. A. Shore, "Polarization dynamics of current-modulated vertical-cavity surface-emitting lasers," *IEEE J. Quantum Electron.* **43**, 1074-1082 (2007).
19. C. Masoller, M. S. Torre and P. Mandel, "Influence of the injection current sweep rate on the polarization switching of vertical-cavity surface-emitting laser," *J. Appl. Phys.* **99**, 026108 (2006).
20. J. Paul, C. Masoller, Y. Hong, P. S. Spencer, and K. A. Shore, "Experimental study of polarization switching of vertical-cavity surface-emitting lasers as a dynamical bifurcation," *Opt. Lett.* **31**, 748-750 (2006).
21. J. Paul, C. Masoller, P. Mandel, Y. Hong, P. S. Spencer, and K. A. Shore, "Experimental and theoretical study of dynamical hysteresis and scaling laws in the polarization switching of vertical-cavity surface-emitting lasers," *Phys. Rev. A* **77**, 043803 (2008).
22. C. E. Preda, B. Segard and P. Glorieux, "Weak temporal ratchet effect by asymmetric modulation of a laser," *Opt. Lett.* **31**, 2347-2349 (2006).
23. M. San Miguel, Q. Feng, and J. V. Moloney, "Light-polarization dynamics in surface-emitting semiconductor lasers," *Phys. Rev. A* **52**, 1728-1739 (1995).
24. J. Martin-Regalado, F. Prati, M. San Miguel and N. B. Abraham, "Polarization properties of vertical-cavity surface-emitting lasers," *IEEE J. Quantum Electron.* **33**, 765-783 (1997).
25. T. Ackemann and M. Sondermann, "Characteristics of polarization switching from the low to the high frequency mode in vertical-cavity surface-emitting lasers," *Appl. Phys. Lett.* **78**, 3574-3576 (2001).
26. C. Masoller and A. S. Torre, "Influence of optical feedback on the polarization switching of vertical-cavity surface-emitting lasers," *IEEE J. Quantum Electron.* **41**, 483-489 (2005).
27. A. Homayounfar and M. J. Adams, "Analysis of SFM dynamics in solitary and optically-injected VCSELs," *Opt. Express* **15**, 10504-10519 (2007).
28. L. Illing and M. B. Kennel, "Shaping current waveforms for direct modulation of semiconductor lasers," *IEEE J. Quantum Electron.* **40**, 445-452 (2004).
29. X. Hachair, S. Barland, J. R. Tredicce, and G. L. Lippi, "Optimization of the switch-on and switch-off transition in a commercial laser," *Appl. Opt.* **44**, 4761-4774 (2005).

1. Introduction

Vertical-cavity surface-emitting lasers (VCSELs) have many characteristics that make them very promising for the next generation of optical networks. They have low threshold current, high power conversion efficiency, high modulation bandwidth, and emit a single-longitudinal-mode at wavelengths of interest for data links and optical fiber technologies [1, 2]. They are compact, have a circular output profile that allows direct fiber coupling, and are easily packaged into two dimensional arrays. VCSELs use DBR mirrors to form a small but highly resonant Fabry Perot cavity. Nowadays photonic-crystal structures are being employed to improve the optical confinement and the mirror reflectivity, resulting in even lower thresholds and smaller cavities with higher Q values [3, 4, 5].

The main drawbacks of VCSELs come from polarization and transverse-mode instabilities [6, 7], and various control methods have been demonstrated, such as the use of a sub-wavelength surface grating locally etched near the optical axis [8]. Because of the polarization-sensitive effective refractive index of the grating structure, one linear polarization has higher reflectivity than the orthogonal one, and because the grating is centrally located, the fundamental transverse mode has higher reflectivity than the higher-order modes. Moreover, sub-wavelength gratings have also great potential for the development of tunable VCSELs [9, 10].

VCSELs can be directly modulated at high speeds and a lot of effort has focused on achieving a small-signal wide modulation bandwidth. Under strong amplitude current modulation nonlinear effects arise (such as period doubling, chaos, multistability, etc. [11, 12, 13]). In VCSELs,

the polarization and transverse-mode competition greatly enhance the complexity of the nonlinear dynamics [14, 15, 16, 17, 18]. Here we propose a novel way to exploit the nonlinearities to generate fast optical pulses using asymmetric triangular modulation, with a modulating signal that is, on average, below the static threshold (the threshold for cw operation).

To the best of our knowledge VCSELs with asymmetric triangular modulation have not been studied so far. Most of previous studies considered sinusoidal modulation; triangular (symmetric) modulation was studied experimentally and numerically in [19, 20, 21], focusing on the influence of the modulation frequency on the polarization-resolved L-I hysteresis curve.

Our work is motivated by a recent experimental and theoretical study using a $\text{Nd}^{3+}:\text{YVO}_4$ diode-pumped laser [22], where asymmetric modulation was applied to the power delivered by the pumping diode laser. It was shown that an asymmetric triangular signal with a slow raising ramp can lead to the emission of pulses, even when the laser is operated, on average, below threshold. In contrast, a signal with a fast raising ramp and the same averaged value does not lead to pulse emission, the intensity remains at the noise level during all the modulation cycle.

In [22] the modulation period was of the order of tens of μs ; here we show that a similar effect can be observed in VCSELs but with much faster modulating signals. The simulations are done using the spin-flip model [23, 24] that has proven to be successful in describing VCSEL dynamics [25, 26, 27]. We show that under suitable modulation parameters subnanosecond pulses on two orthogonal linear polarizations can be obtained even through the injection current is, on average, below the cw threshold. We interpret the results as due to the nonlinear interplay of the optical field and the carrier density in the active medium.

The method proposed here for the generation of optimal pulses with low average injection current via asymmetric modulation is based on exploiting the nonlinear light-matter interaction, and from this point of view, is similar to the methods proposed in [28, 29], for optimizing the performance of directly modulated semiconductor lasers by shaping the current input. Appropriate square-shaped current inputs allow to control the laser time-evolution in the plane (photon density, carrier density). In [28] the aim was to avoid dynamical memory effects that arise because even if the observable intensity has returned to its stationary value after a current waveform was applied, the unobservable carrier density may not have reached its stationary value. By suppressing dynamical memory effects the laser output is not influenced by previously communicated information, which improves its performance in digital data communication systems. In [29] adequate square-shaped injection current inputs were demonstrated numerically and experimentally, to switch on a semiconductor laser without relaxation oscillations (first a large pump value was applied to speed up the switch-on, followed by a lower value, temporarily below threshold, tailored to eliminate just the right amount of the accumulated carriers, whose excess would otherwise cause damped relaxation oscillations).

This paper is organized as follows: Section 2 presents the model employed, Section 3 presents the results of the simulations, characterizing the influence of various asymmetric modulation parameters, and Section 4 presents a summary and the conclusions.

2. Model

The spin-flip rate equations for the orthogonal linearly polarized slowly-varying amplitudes, E_x and E_y , the total carrier density, $N = N_+ + N_-$, and the carrier difference, $n = N_+ - N_-$ (N_+ and N_- being populations with opposite spin) are [23, 24]:

$$\frac{dE_{x,y}}{dt} = k(1 + i\alpha)[(N - 1)E_{x,y} \pm inE_{y,x}] \mp (\gamma_a + i\gamma_p)E_{x,y} + \sqrt{\beta_{sp}}\xi_{x,y}, \quad (1)$$

$$\frac{dN}{dt} = \gamma_N[\mu(t) - N(1 + |E_x|^2 + |E_y|^2) - in(E_yE_x^* - E_xE_y^*)], \quad (2)$$

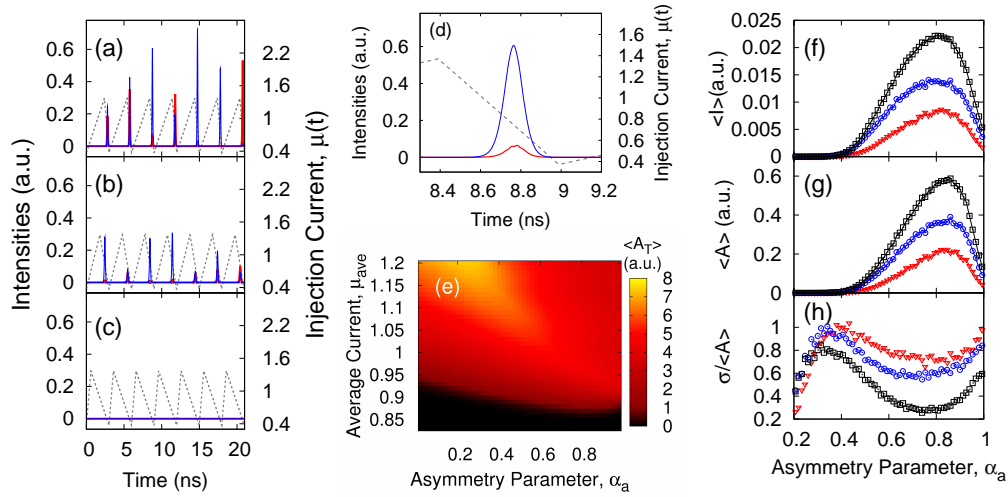


Fig. 1. Time traces of the intensities of the orthogonal linear polarization: I_x (red), I_y (blue), and the injection current $\mu(t)$ (dashed) for an asymmetry parameter (a) $\alpha_a=0.8$, (b) 0.6 and (c) 0.2. (d) Detail of a pulse in Fig.1(a). (e) Color plot of the average pulse total amplitude, $\langle A_T \rangle$, for a fixed modulation amplitude, $\Delta\mu=1$. (f) and (g) Time averaged intensities, $\langle I \rangle$, and pulse amplitudes, $\langle A \rangle$, respectively (x polarization (red), y polarization (blue) and total intensity (black)). (h) Normalized standard deviation, $\sigma/\langle A \rangle$, of the pulse amplitude vs. the asymmetry parameter, α_a . The modulation amplitude is $\Delta\mu=1$, the period is $T=3$ ns. The DC value $\mu_0=0.37$ is fixed in captions (a)-(d) and (f)-(g) and is varied in (e).

$$\frac{dn}{dt} = -\gamma_s n - \gamma_N [n(|E_x|^2 + |E_y|^2) + iN(E_y E_x^* - E_x E_y^*)], \quad (3)$$

where k is the field decay rate, γ_N is the decay rate of the total carrier population, γ_s is the spin-flip rate which accounts for the mixing of carrier populations with different spins, α the linewidth enhancement factor, γ_a and γ_p are linear anisotropies representing dichroism and birefringence, β_{sp} is the noise strength, $\xi_{x,y}$ are uncorrelated Gaussian white noises and $\mu(t)$ is the normalized injection current parameter: the static cw threshold is at $\mu_{th,s} = 1$.

The current is modulated with an asymmetric triangular signal of amplitude $\Delta\mu$, rising from μ_0 a time interval T_1 and falling back to μ_0 a time interval T_2 . One modulation cycle is: $\mu(t) = \mu_0 + \Delta\mu (t/T_1)$ for $0 \leq t \leq T_1$, $\mu(t) = \mu_0 + \Delta\mu [1 - (t - T_1)/T_2]$ for $T_1 \leq t \leq T_1 + T_2$. The average current, $\mu_{ave} = \mu_0 + \Delta\mu/2$, is independent of the modulation period, $T = T_1 + T_2$. The asymmetry of the modulation is characterized by the parameter $\alpha_a = T_1/T$ with $0 \leq \alpha_a \leq 1$.

3. Results

The equations were simulated with typical VCSEL parameters [24]: $k = 300 \text{ ns}^{-1}$, $\alpha = 3$, $\gamma_N = 1 \text{ ns}^{-1}$, $\gamma_a = 0.5 \text{ ns}^{-1}$, $\gamma_p = 50 \text{ rad/ns}$, $\gamma_s = 50 \text{ ns}^{-1}$, and $\beta_{sp} = 10^{-6} \text{ ns}^{-1}$.

Current modulation leads to the emission of optical pulses even when, on average, the injection current is below the cw threshold. The intensity is emitted in irregular pulses in both linear polarizations. Figures 1 (a)-(d) display time traces of $I_x = |E_x|^2$ and $I_y = |E_y|^2$ for three modulation asymmetries and the same average current value, $\mu_{ave} = 0.87 < 1$. The modulation period and amplitude are chosen such that the laser emits only one pulse per modulation cycle.

It can be observed that with slow-rising and fast-decreasing ramps, Fig. 1(a), the laser emits larger pulses than with a more symmetric signal, Fig. 1(b). In contrast, with fast-rising and

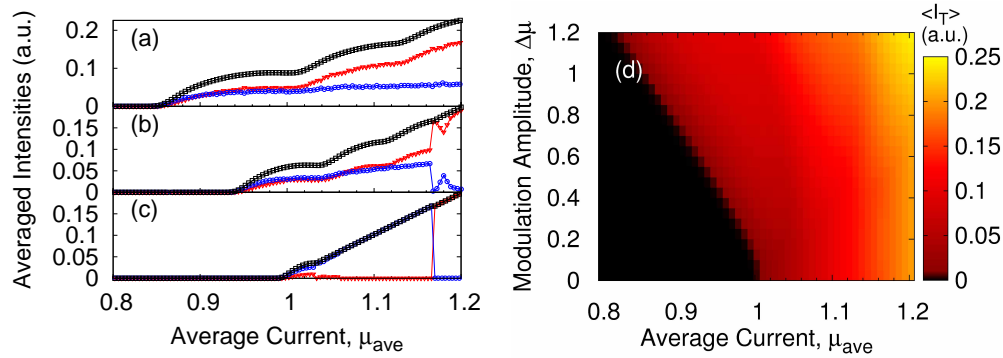


Fig. 2. (a)-(c) Time averaged intensities [x polarization $\langle I_x \rangle$ (red), y polarization $\langle I_y \rangle$ (blue) and total intensity $\langle I_T \rangle$ (black)] vs. average current, μ_{ave} , for different modulation amplitudes (a) $\Delta\mu=1.0$, (b) 0.5, and (c) 0.15. (d) Color plot of average total intensity $\langle I_T \rangle$. The asymmetry parameter $\alpha_a=0.8$ and the period $T=3$ ns are fixed.

slow-decreasing ramps, Fig. 1(c), the laser does not turn on, in agreement with Ref.[22].

Figure 1(f) displays the time averaged intensities, $\langle I_x \rangle$, $\langle I_y \rangle$ and $\langle I_T \rangle = \langle I_x + I_y \rangle$; Fig. 1(g) displays the time averaged pulse amplitudes, $\langle A_x \rangle$, $\langle A_y \rangle$ and $\langle A_T \rangle$ (when there is more than one pulse per modulation cycle, we calculate the average amplitude of the largest pulse). The amplitudes are one order of magnitude larger than the intensities because the laser emits sharp pulses and is off during most of the modulation cycle. Figure 1(h) displays the dispersion of the amplitude of the pulses, characterized in terms of the standard deviation normalized to the mean value. There is an optimal modulation asymmetry, typically $\alpha_a \cong 0.8$, for which the averaged intensity and the averaged pulse amplitude reach their maximum value, and for this asymmetry the dispersion of the pulse amplitude reaches its minimum value.

For the optimal asymmetry a pulse is emitted just at the end of the modulation cycle, as can be seen in Fig. 1(d). This is also in good agreement with the observations of [22], and can be interpreted, as in [22], as due to the nonlinear interplay of the photons and the carriers in the active region. Two mechanisms trigger the emission of a pulse: spontaneous emission and the radiation left by the previous pulse. When the radiation left by the previous pulse is absorbed by the carriers during the fall part of the cycle, spontaneous emission is the dominant mechanism for triggering the next pulse in the next cycle. On the contrary, when the radiation left by the previous pulse has not been completely absorbed, it dominates over spontaneous emission for triggering the next pulse.

The "effective" lasing threshold depends on the asymmetry of the modulation as can be seen in Fig. 1(e), that displays a color-coded 2D plot of the averaged amplitude of the pulses of the total intensity, $\langle A_T \rangle$, vs. α_a and μ_0 , for fixed modulation amplitude [$\Delta\mu$ is the same as in Figs. 1(f)-(h), thus, Fig. 1(f)-(h) are an horizontal scan in Fig. 1(e)]. In the vertical axis of Fig. 1(e) μ_{ave} is plotted instead of μ_0 ($\mu_{ave} = \mu_0 + \Delta\mu/2$) to show explicitly that the laser emits pulses even when the average current is below the cw threshold. $\langle A_T \rangle$ increases with μ_{ave} , and the relation is nonlinear, as will be discussed below. For the optimal asymmetry that leads to maximum pulse amplitude with $\mu_{ave} < 1$ ($\alpha_a \cong 0.8$), there is also the largest effective threshold reduction. In contrast, for modulations on average above the cw threshold, the optimal asymmetry to obtain maximum pulse amplitude is such that $\alpha_a < 0.5$ [yellow region in the top-left corner of Fig. 1(e)], i.e., the modulation has a fast rising ramp followed by a slow decreasing one.

The "effective" threshold depends also on the modulation parameters μ_0 and $\Delta\mu$. Figures

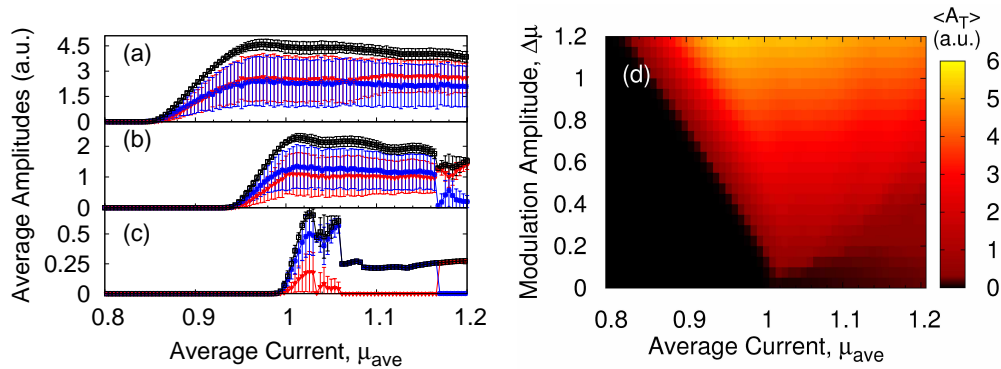


Fig. 3. (a)-(c) Time averaged pulse amplitudes [x polarization $\langle A_x \rangle$ (red), y polarization $\langle A_y \rangle$ (blue) and total amplitude $\langle A_T \rangle$ (black)] vs. average current, μ_{ave} , for different modulation amplitudes (a) $\Delta\mu=1.0$, (b) 0.5, and (c) 0.15. (d) Color plot of the average total intensity, $\langle I_T \rangle$. Parameters are as in Fig. 2.

2(a)-(c) show the averaged intensities, $\langle I_x \rangle$, $\langle I_y \rangle$ and $\langle I_T \rangle$, for $\alpha_a = 0.8$ and three values of $\Delta\mu$. In each caption $\Delta\mu$ and α_a are kept fixed while μ_0 varies, but in the horizontal axis we plot μ_{ave} instead of μ_0 to show that, for large $\Delta\mu$ and small μ_0 , there is laser emission with $\mu_{ave} < 1$. $\langle I_T \rangle$ increases with μ_{ave} , and for large $\Delta\mu$, Figs. 2(a), 2(b), the relation is nonlinear; kinks appear which are due to the emission of additional pulses in each modulation cycle.

The variation of the effective threshold with both, μ_0 and $\Delta\mu$, is illustrated in Fig. 2(d), that presents a color-coded 2D plot of $\langle I_T \rangle$. Also here the horizontal axes displays μ_{ave} instead of μ_0 , and Figs. 2(a)-(c) correspond to horizontal scans in 2(d). In the bottom-left corner of Fig. 2(d), $\Delta\mu$ and/or μ_0 are too small, and the laser does not turn on, the black color representing the intensity at the noise level. We observe a smooth turn-on: as $\Delta\mu$ and/or μ_0 increase, $\langle I_T \rangle$ gradually increases.

Figure 3 displays the time averaged pulse amplitude, $\langle A_T \rangle$, for the same parameters as Fig. 2. It can be noticed that near the effective threshold $\langle A_T \rangle$ increases nearly linearly with μ_{ave} , while for larger μ_{ave} , $\langle A_T \rangle$ saturates but $\langle I_T \rangle$ continues increasing with μ_{ave} , as seen in Fig. 2. This is due to the fact that the laser emits more than one pulse per modulation cycle.

4. Conclusion

The dynamics of a VCSEL driven by asymmetric triangular current modulation was studied numerically using the spin-flip model. When the injection current is, on average, below the cw threshold irregular optical pulses in two orthogonal linear polarizations can be generated by using large amplitude modulation of period of a few nanoseconds. For an optimal modulation asymmetry, with a slow rising ramp followed by a fast decreasing one, the effective threshold reduction is about 20%, the pulse amplitude is maximum and the dispersion of the pulse amplitude is minimum. In contrast, when the averaged current value is above the static threshold, the optimal modulation asymmetry that leads to maximum pulse amplitude has a fast rising ramp followed by a slow decreasing one.

Acknowledgment

This research was supported by AFOSR grant FA9550-07-1-0238. CM acknowledges support from the ‘‘Ramon y Cajal’’ Program (Spain) and the Spanish Ministerio de Educacion y Ciencia through project FIS2005-07931-C03-03.